Available online at www.sciencedirect.com
ScienceDirect
International Journal of Pharmaceutics 324 (2006) 56–66
INTERNATIONAL JOURNAL OF PHARMACEUTICS
www.elsevier.com/locate/ijpharm

Pharmaceutical Nanotechnology

Nanoscopic core-shell drug carriers made of amphiphilic triblock and star-diblock copolymers

Fabiana Quaglia [a,*], Luisanna Ostacolo [a], Giuseppe De Rosa [a], Maria Immacolata La Rotonda [a], Massimo Ammendola [b], Giuseppe Nese [b], Giovanni Maglio [b], Rosario Palumbo [b], Christine Vauthier [c]

[a] *Department of Pharmaceutical and Toxicological Chemistry, University of Napoli Federico II, Via D. Montesano 49, 80131 Napoli, Italy*
[b] *Department of Chemistry, University of Napoli Federico II, Via Cinthia, 80126 Napoli, Italy*
[c] *Laboratoire de Physico-chimie, Pharmacotechnie et Biopharmacie, UMR CNRS 8612, Université de Paris Sud, 5 Rue J.B. Clément, 92296 Chatenay-Malabry Cedex, France*

Received 17 February 2006; received in revised form 9 July 2006; accepted 13 July 2006
Available online 16 July 2006

Abstract

The aim of this work was to design injectable nanocarriers for drug delivery based on PCL–PEO amphiphilic block copolymers with linear ABA triblock and 4-armed $(BA)_4$ star-diblock architectures (A = PEO, B = PCL). The copolymers were obtained by coupling of a monofunctional –COOH end-capped PEO (M_n = 2.0 kDa) with linear or 4-armed star-shaped PCL macromers bearing –OH terminal groups and were characterized by ^{1}H NMR spectroscopy and size exclusion chromatography. DSC and X-ray diffraction experiments showed that separate crystalline phases of PCL and PEO are present in bulk copolymers. Nanoparticles were produced by nanoprecipitation (NP) and by a new melting-sonication procedure (MS) without the use of toxic solvents, and characterized for size, polydispersity, zeta potential and core-shell structure. Nanoparticles were loaded with *all-trans*-retinoic acid (*at*RA) as a model drug and their release features assessed. Results demonstrate that both techniques allow the formation of PEO-coated nanoparticles with a hydrodynamic diameter that is larger for nanoparticles prepared by MS. *at*RA is released from nanoparticles at controlled rates depending on size, loading and, more important, preparation technique, being release rate faster for MS nanoparticles. Some biorelevant properties of the carrier such as complement activation were finally explored to predict their circulation time after intravenous injection. It is demonstrated that nanoparticles prepared by MS do not activate complement and are of great interest for future *in vivo* applications.

Keywords: Nanoparticles; Amphiphilic block copolymers; Poly(epsilon-caprolactone); Poly(ethylene oxide); *All-trans*-retinoic acid

1. Introduction

With the remarkable development of nanomedicine in recent years, new drug delivery approaches based on the state-of-the-art nanotechnology have been receiving significant attention (Emerich and Thanos, 2003; Moghimi et al., 2005; Couvreur and Vauthier, 2006). Such process involves the identification of precise targets (cells and receptors) related to specific clinical conditions and choice of the appropriate nanocarrier to achieve the required response while minimizing the side effects. Rational approaches in design and surface engineering of nanoscale systems are generally needed to impart suitable biological properties as well as optimized technological features. Nanocarriers for anticancer targeting, for example, should be long-circulating to escape the reticular endothelial system (RES) and able to extravasate in the target organs making advantage of enhanced permeability and retention (EPR) effect (Kim and Lim, 2002; Brannon-Peppas and Blanchette, 2004; Jain, 2005; Reddy, 2005; Vasir and Labhasetwar, 2005).

In their simplest design, long-circulating nanoparticles are formed by a solid core, made of biodegradable polymers, and a hydrophilic corona, made of flexible hydrophilic chains. Hydrophobic biodegradable core contains the drug, which is protected from *in vivo* inactivation, and controls drug release rate. Hydrophobic blocks generally originates from poly(lactic acid), poly(lactic-*co*-glycolic acid) and poly(alkylcyanoacrylate), although recently a renewed attention has been paid to poly(ε-caprolactone) (PCL). The presence of

* Corresponding author. Tel.: +39 081678707; fax: +39 081678707.
E-mail address: quaglia@unina.it (F. Quaglia).

0378-5173/$ – see front matter © 2006 Elsevier B.V. All rights reserved.
doi:10.1016/j.ijpharm.2006.07.020

a hydrophilic coating offers steric stabilization toward aggregation "in the bottle" while also dictating the pharmacokinetics and biodistribution of the carrier. A number of reviews are available where it is well illustrated how surface modification can be carried out to obtain long-circulating nanoparticles, making use of poly(ethylene oxide) (PEO) (Bhadra et al., 2002; Otsuka et al., 2003) or more recently polysaccharides (Lemarchand et al., 2003, 2004; Labarre et al., 2005). Core-shell nanocarriers can be obtained either by coating the hydrophobic core with hydrophilic polymers/surfactants or designing tailor-made block copolymers (Soppimath et al., 2001).

Amphiphilic block copolymers represent a large family of materials consisting of ordered sequences of two or more different monomers connected by chemical bonds and arranged with different architectures (Kumar et al., 2001; Qiu and Bae, 2006). In the simplest case a diblock copolymer AB consists of two different homopolymers linked end to end. Extension of this concept leads to ABA or BAB triblocks, $(AB)_n$ linear multiblocks and to radial arrangements of block copolymers, the simplest case being that of star-shaped structures, where *n* block copolymer chains are linked by one of their ends to a multifunctional moiety. Another structural possibility designated by heteroarm block copolymers is to link *n* homopolymer sequences to a given junction point. Resulting block copolymers can be used to form nanoparticles or micelles by different methods which are generally selected depending on copolymer solubility and drug features.

Among poly(ester)/PEO copolymers, diblock architecture is generally preferred to produce core-shell carriers. A number of papers have highlighted how PEO length and surface density can affect biomimetic properties of the nanocarrier, with special regard to opsonization process and *in vivo* fate (Gref et al., 2000; Kim et al., 2005). On the other hand very few is known about the applicability of novel polymer architectures in core-shell nanocarrier development, where they have the potential to offer a superior degree of nanoparticle coating.

Our aim was to develop PEO-coated nanocarriers for intravenous administration made of PCL–PEO amphiphilic block copolymers with linear ABA triblock and 4-armed $(BA)_4$ star-shaped architectures (A = PEO, B = PCL). The feasibility of producing nanoparticles by a novel melting-sonication procedure without the use of toxic solvents was explored too. To assess loading capacity of the nanoparticles, *all-trans*-retinoic acid (*at*RA) was employed as a model drug. Some biorelevant properties of the nanocarrier with special regard to complement activation were finally assessed to predict their ability to escape the RES.

2. Materials and methods

2.1. Reagents and materials

ε-Caprolactone, CL (Aldrich) was distilled from CaH_2 under vacuum. Pentaerythritol, PERT (Fluka) was purified by vacuum sublimation at 200 °C. Tin(2-ethylhexanoate)$_2$, Sn(oct)$_2$, (Aldrich), 4-(dimethylamino)pyridine, DMAP, (Fluka) and 1,3-dicyclohexylcarbodiimide, DCC (Fluka) were used as received. *N*,*N*′-dimethylformamide, DMF, and dichlorometane, DCM (Aldrich) were dried before use. Monomethoxy poly(ethylene glycol) with $M_n = 2.0$ kDa, *m*-PEO$_{2.0}$ (Aldrich) was dried by distillation from toluene of the water–toluene azeotrope. α-Methoxy-ω-carboxymethyl-PEO, *m*-PEO$_{2.0}$–COOH was obtained reacting *m*-PEO$_{2.0}$ with succinic anhydride as previously reported (Maglio et al., 2004). *All-trans*-retinoic acid (*at*RA), potassium phosphate dibasic and potassium phosphate monobasic were from Sigma–Aldrich. Analytical grade acetone, ethanol and tetrahydrofuran (THF) were from Carlo Erba Reagenti (Italy).

2.2. Synthesis of a linear PCL macromer (l-PCL$_{6.7}$)

CL (30.0 g, 263 mmol), 1,4-butanediol (0.394 g, 4.38 mmol) and 0.018 g (0.044 mmol) of Sn(oct)$_2$ (molar ratio: Sn/OH 1/200, CL/OH 60/1) dissolved in 0.22 ml of CL were charged in a flame dried vial under dry nitrogen. The vial was sealed under vacuum and heated at 140 °C for 24 h. After cooling to room temperature, the vial was opened and the polymer was dissolved in DCM (110 ml) and precipitated in 600 ml of methanol at 0 °C (26.9 g, 88% yield; $\eta_{inh} = 0.32$ dl/g; $CHCl_3$, 25 °C, $C = 0.5$ g/dl).

2.3. Synthesis of a 4-arm PCL star-shaped macromer (s-PCL$_{19.6}$)

PERT (0.259 g, 1.90 mmol) was dissolved at 105 °C under dry nitrogen atmosphere in 38.1 g (334 mmol) of CL and 4.75 ml of DMF. A 0.25 M solution of Sn(oct)$_2$ in DMF (0.15 ml, 0.038 mmol of Sn) was added to the reaction mixture and the polymerisation was carried out under stirring at 105 °C for 48 h (molar ratio: Sn/OH 1/200, CL/OH 43.9/1). The DMF was removed under vacuum and the residue was dissolved in chloroform and precipitated in methanol at 0 °C to give s-PCL$_{19.6}$ (37.6 g, 98% yield; $M_n = 19.6$ kDa as determined by ^{1}H NMR; $\eta_{inh} = 0.34$ dl/g; $CHCl_3$, 25 °C, $C = 0.5$ g/dl).

2.4. Synthesis of linear triblock and star-shaped diblock PCL–PEO copolymers

The coupling of PCL macromers with *m*-PEO$_{2.0}$–COOH was performed as previously reported (Maglio et al., 2004). The synthesis of s-PCL$_{19.6}$–PEO$_{2.0}$ is reported as an example. Briefly: a solution of DCC (1.26 mmol) in 5 ml of DCM and a solution of s-PCL$_{19.6}$ (0.25 mmol) in 10 ml of DCM were added under stirring to *m*-PEO$_{2.0}$–COOH (1.05 mmol) and DMAP (0.25 mmol) dissolved in 13 ml of DCM, under dry nitrogen atmosphere, and the reaction was carried for 48 h at room temperature. After purification, s-PCL$_{19.6}$–PEO$_{2.0}$ was obtained with 80% yield ($\eta_{inh} = 0.46$ dl/g, $CHCl_3$, 25 °C, $C = 0.5$ g/dl). The coupling of l-PCL with *m*-PEO$_{2.0}$–COOH to give l-PCL$_{6.7}$–PEO$_{2.0}$ was performed as above (70% yield; $\eta_{inh} = 0.38$ dl/g; $CHCl_3$, 25 °C, $C = 0.5$ g/dl).

2.5. Polymer characterization

The inherent viscosities were measured in chloroform at 25 °C using an Ubbelohde viscometer ($C = 0.5$ g/dl). Differential

scanning calorimetry (DSC) analyses were performed on a Mettler 30 calorimeter under nitrogen using a 2 °C/min scan rate. Samples were heated from 0 to 80 °C, cooled at 0 °C and finally heated again to 80 °C. Glass transition temperatures were determined heating at 10 °C/min samples previously quenched at −100 °C. Wide-angle X-ray scattering (WAXS) diagrams were recorded at 20 °C on a Philips PW-1711 diffractometer using a Ni-filtered Cu Kα radiation (1.5418 Å). The crystallinity degree was evaluated subtracting the contribution of the amorphous part from the total scattering. Size exclusion chromatography (SEC) analyses were performed in THF at 20 °C using two Phenogel columns (5 μm, 500 and 1000 Å, 300 mm × 7.8 mm from Phenomenex, USA) connected in series to a RI detector by using polystyrene standards. Optical microscopy was performed on a Axioscop-Zeiss instrument equipped with a THMS 600 hot stage and a Linkam TMS 91 temperature programmer. ^{1}H NMR spectra were recorded at 25 °C with Varian Gemini 200 or 300 instruments at 200 or 300 MHz, respectively, using chloroform-*d* as solvent. Spectra of nanoparticles in D_2O were recorded using samples obtained either by melt sonication in D_2O or by precipitation of acetone-d_6 solutions of copolymers in D_2O.

2.6. Preparation of unloaded nanoparticles

Nanoparticles were prepared by both a classic nanoprecipitation technique (Fessi et al., 1986) and a novel melting/sonication procedure. Nanoprecipitation was conducted by dissolving 20 mg of copolymer in 2 ml of acetone and adding this solution dropwise (0.07 ml/min) to 4 ml of water under magnetic stirring. After 30 min, acetone was completely evaporated under vacuum. In the melting-sonication procedure, 20 mg of copolymer were added to 4 ml of filtered water in a vial, poured in a oil bath heated at 72 ± 2 °C to allow copolymer melting, sonicated for 10 min at 18 W (Sonicator 3000, Misonix, USA) by a microtip probe and finally cooled at room temperature. In both cases, nanoparticles were filtered through 0.45 μm filters (RC, Chemtek, Italy) and kept at 4 °C.

Recovery yield of nanoparticles was evaluated by freeze-drying 0.2 ml of each formulation and weighting the solid residue. Results are expressed as the ratio of the actual nanoparticle weight to the theoretical polymer weight × 100.

2.7. Preparation of atRA-loaded nanoparticles

For the preparation of *at*RA-loaded nanoparticles by nanoprecipitation, 20 mg of copolymer and 2 mg of *at*RA were dissolved in 2 ml of acetone and precipitated in 4 ml of water. For the preparation of *at*RA-loaded nanoparticles by melting-sonication, 2 mg of drug were dissolved in 0.4 ml of ethanol (5 mg/ml), added to 3.6 ml of filtered water in the presence of 20 mg of copolymer previously molten at 72 ± 2 °C and sonicated. In both cases, nanoparticles were filtered through 0.45 μm filters (RC, Chemtek, Italy). Stability of *at*RA in the experimental conditions realized to prepare nanoparticles by melting sonication were evaluated by HPLC (Shimadzu) on a Gemini 5 μm C_{18} column (250 mm × 4.6 mm) with UV detection at 352 nm. Mobile phase was a mixture methanol/water 90:10 (v/v) and flow rate 1 ml/min. A control *at*RA solution in water gave the same signals and intensity ratios as compared to that treated by melting/sonication.

2.8. Characterization of nanoparticles

The hydrodynamic diameter of the nanoparticles was determined by photon correlation spectroscopy using a N5 Submicron Particle Size Analyzer (Beckman-Coulter). Nanoparticle dispersion was suitably diluted in Milli-Q water at the optimal intensity (about 9×10^5 counts/s). Measurements were performed at 25 °C on 90° angle. The morphology of nanoparticles was assessed by transmission electron microscopy (TEM) on a LEO 912AB (Zeiss). Nanoparticle suspension was stained with uranile acetate (4% w/v) and mounted on nichel grids. Zeta potential of the nanoparticles was determined on a Zetasizer Nano Z (Malvern Instruments Ltd.) in 0.02 M phosphate buffer at pH values of 3.0 and 6.5. Results are reported as mean of three separate measurements on three different batches ($n = 9$) ± standard deviation.

For *at*RA loaded nanoparticles, encapsulation efficiency and release rate were assessed. *at*RA loading was determined by dissolving a known amount of freeze-dried nanoparticles in THF and evaluating UV absorbance of the solution at 352 nm (UV-1200, Shimadzu). To verify a possible interference of copolymers, an amount of unloaded nanoparticles was dissolved in THF. No UV absorption at 352 was found. Release profiles of *at*RA from nanoparticles were evaluated by dialysis placing 1.5 ml of nanoparticles suspension in a dialysis sac (molecular weight cut-off 3500 Da, Spectrapor) using a 10 mM phosphate buffer at pH 7.4 (10 ml) and 37 °C as release medium. At predetermined intervals, 1 ml of medium was withdrawn and replaced by the same amount of fresh buffer. *at*RA was quantified by UV as described above. As control, dissolution profile of nanoprecipitated *at*RA was assessed too. In all cases, sink conditions were realized.

2.9. Evaluation of complement activation by 2D-immunoelectrophoresis of C3

Complement activation was assessed in human serum following the protocol by Labarre et al. (2005). Its activation in the presence of different nanoparticles was evidenced by evaluating conversion of C3 into C3b by 2D-immunoelectrophoresis using a polyclonal antibody to detect both C3 (non-activated complement) and C3b (activated complement).

Human serum was obtained after calcifying plasma from healthy donors and stored at −80 °C until use. To ensure a valid comparison of the formulations, nanoparticle samples with a comparable surface area (1000 cm^2) were tested. A nanoparticle suspension (about 200 μl) was incubated under gentle agitation for 1 h at 37 °C with 100 μl human serum and 100 μl Veronal-buffered saline containing 0.15 mM Ca^{2+} and 0.5 mM Mg^{2+} ions (VBS^{2+}). After incubation, 5 μl of each sample were subjected to a first electrophoresis on 1% agarose gel. The second-dimension electrophoresis was carried out on Gelbonds® films (Cambrex) in agarose gel plates (1%) containing a polyclonal antibody to

human C3 (Complement C3 antiserum rose in goat, Sigma), recognizing both C3 and C3b. The films were finally dried and stained with Coomassie blue to reveal the presence of C3 and C3b which have reacted with the antibody. Serum diluted in VBS-EDTA (1/4 v/v) was used as negative control of complement activation. Serum diluted in VBS^{2+} was used as control of the spontaneous activation of complement occurring in the experimental conditions used. Sephadex G 25 superfine (Pharmacia) incubated in serum diluted in VBS^{2+} was used as a positive control. Each nanoparticle formulation was analysed three times across the whole process.

3. Results and discussion

3.1. Synthetic strategies to prepare amphiphilic PCL–PEO block copolymers

Linear ABA triblock and 4-armed $(BA)_4$ star-shaped diblock copolymers, both consisting of hydrophilic PEO A blocks and hydrophobic PCL B blocks, were selected as models of amphiphilic copolymers suitable for applications as nanosized drug carriers considering: (i) the biocompatibility of both blocks; (ii) the high hydrophobicity and flexibility of PCL segments; (iii) the copolymer architectures characterized by inner PCL and outer PEO blocks. The copolymers were synthesized according to the pathway outlined in Scheme 1. Linear and star-shaped PCL macromers with two and four –OH end groups, respectively, were obtained in the first step and then coupled with monofunctional *m*-$PEO_{2.0}$–COOH in a second coupling step.

3.2. Synthesis and characterization of linear and star-shaped PCL macromers

A linear, dihydroxy-terminated PCL macromer having $M_n = 6.7$ kDa (l-$PCL_{6.7}$), was obtained by the ring-opening polymerisation (ROP) of CL at 130 °C using 1,4-butanediol as initiator and a catalytic amount of $Sn(oct)_2$. The M_n was calculated according to the following equation:

$$M_n = \left[\left(\frac{2b}{a}\right) 114\right] + 90$$

where a and b are the intensities of the resonance associated to –CH_2–OH methylene protons (a) at 3.64 δ and to –CH_2–CO– units in the PCL chain (b) at 2.31 δ in the ^{1}H NMR spectrum and 90 and 114 are the molecular masses of the initiator and of the PCL chain repeat unit, respectively. A monomodal molecular weight distribution with a polydispersity index (PDI = M_w/M_n) of 1.50 was found by SEC for l-$PCL_{6.7}$. A four-armed star-shaped PCL macromer (s-PCL) was synthesized by a divergent method using a tetrafunctional alcohol, PERT, as initiator under experimental conditions similar to those described for l-$PCL_{6.7}$, but using DMF as a solvent to increase the solubility of the initiator in the reaction medium and to enhance the accessibility of –OH groups of PERT in the initiation step. Using a CL/OH molar ratio of 44 a star-shaped PCL macromer with $M_n = 19.6$ kDa and PDI = 1.30 (s-$PCL_{19.6}$), was obtained and employed in the synthesis of an amphiphilic 4-armed copolymer. The s-$PCL_{19.6}$ macromer had a highly regular structure characterized by an effective number of arms of 3.8, quite close to the theoretical

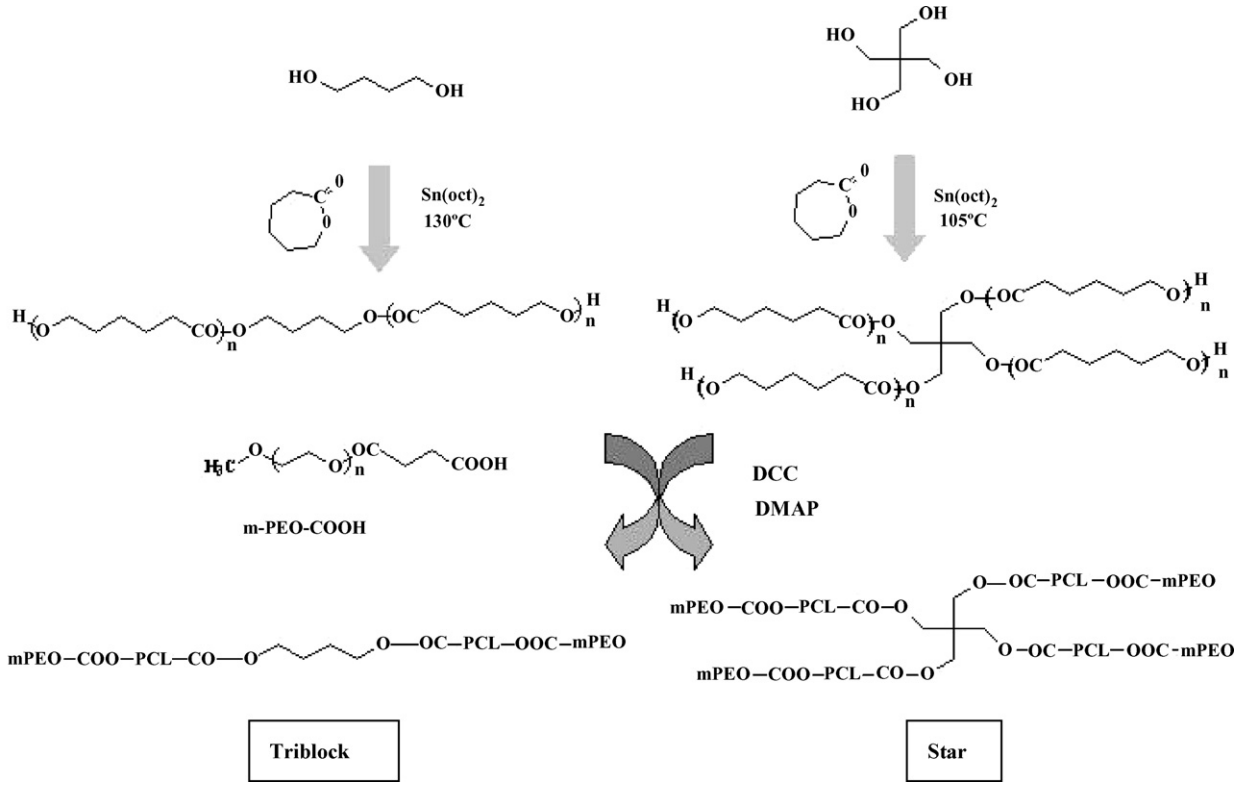

Scheme 1. Reaction pathways for the synthesis of triblock and star-diblock poly(ε-caprolactone)/poly(ethylene oxide) copolymers.

Table 1
Linear and star-shaped PCL macromers and their copolymers with $PEO_{2.0}$

Polymer code	$M_{n\,(theor)}$ (kDa)[a]	$M_{n\,(exp)}$ (kDa)[a]	Yield (%)	η_{inh} (dl/g)[b]	φ (%)[c]	PDI[d]
l-$PCL_{6.7}$	–	6.7	88	0.32	–	1.50
s-$PCL_{19.6}$	–	19.6	98	0.34	–	1.30
l-$PCL_{6.7}$–$(PEO_{2.0})_2$	10.9	10.8	70	0.38	95	1.32
s-$PCL_{19.6}$–$(PEO_{2.0})_4$	28.0	27.3	72	0.46	97	1.23

[a] Number-average molecular weight theoretical (theor) and calculated from ^{1}H NMR spectra (exp).
[b] Inherent viscosity in $CHCl_3$ at 25 °C, $C = 0.5$ g/dl.
[c] Efficiency of the coupling reaction calculated by ^{1}H NMR spectroscopy.
[d] Polydispersity index evaluated by SEC.

value of 4, as assessed by ^{1}H NMR spectroscopy (Maglio et al., 2004).

3.3. Synthesis and characterization of PEO–PCL–PEO triblock and PCL–PEO star-diblock copolymers

The amphiphilic PEO–PCL–PEO triblock and PCL–PEO star-diblock copolymers were obtained by reacting the –OH end-capped l-$PCL_{6.7}$ and s-$PCL_{19.6}$ macromers with monofunctional *m*-$PEO_{2.0}$–COOH to form ester linkages between the PCL and PEO segments. *m*-$PEO_{2.0}$–COOH was prepared reacting the –OH end group of *m*-$PEO_{2.0}$ with succinic anhydride. The coupling was performed in DCM using DCC and DMAP as a carboxyl group activating agent and as a catalyst, respectively. The results of the coupling reaction are reported in Table 1 together with the characterization data of PCL macromers. The reaction efficiency of the coupling (φ) was higher than 95%, as assessed by ^{1}H NMR spectroscopy comparing the integrals of $–CH_2–O–CH_2–$ resonance (PEO) at 3.6–3.7 δ with those of $–CH_2–OCO–$ resonance at 4.07 δ (PCL). The molar mass distributions of the triblock and star-diblock copolymers were relatively narrow with PDI values (1.32 and 1.23, respectively), slightly lower than those of the corresponding l-$PCL_{6.7}$ and s-$PCL_{19.6}$ precursors.

The thermal properties and the crystallization behaviour of the PCL macromers and of the copolymers were investigated by DSC and X-ray diffraction analysis and the results are reported in Table 2. Single glass transitions, determined after a quenching step from 100 to −100 °C, were found at −62 °C for s-$PCL_{19.6}$–$(PEO_{2.0})_4$ and at −58 °C for l-$PCL_{6.7}$–$(PEO_{2.0})_2$, values very close to the T_g of the precursor macromers, both characterized by high segmental mobility. Typical DSC thermograms are shown in Fig. 1. The melting and crystallization temperatures of s-PCL and l-PCL macromers (traces a and c) are very close each other as expected taking in account that T_m increases with increasing the chain length which is slightly higher for s-$PCL_{19.6}$, but decreases with branching because chain ends act as structural defects. The star-like architecture is responsible for the slightly lower values of crystallinity indicated both by ΔH_m and X_c for s-$PCL_{19.6}$ as compared to l-$PCL_{6.7}$. The DSC thermograms of the copolymers (traces b and d) exhibited two well separated melting endotherms, both in first and second heating runs, as well as two crystallization exotherms in

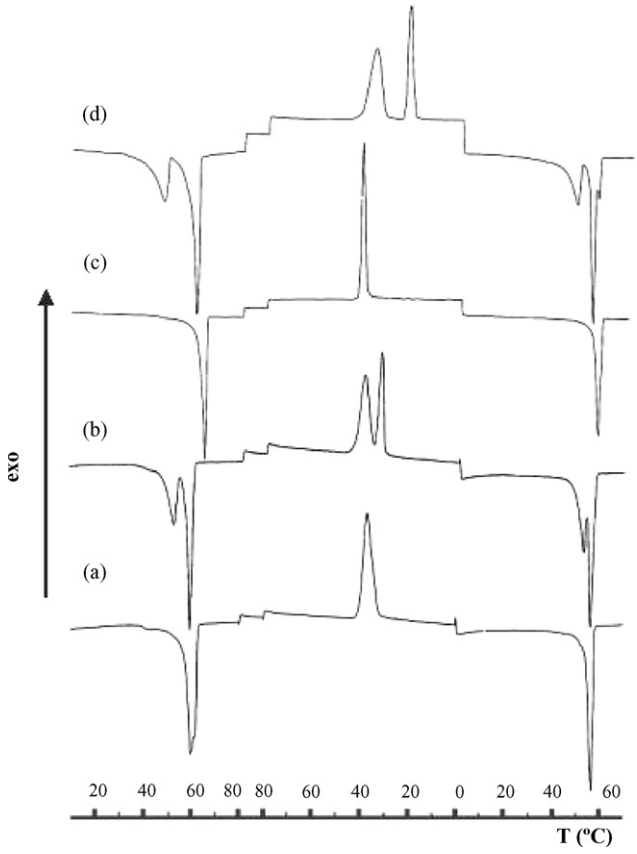

Fig. 1. DSC thermograms of s-$PCL_{19.6}$ (a) and l-$PCL_{6.7}$ (c) macromers and s-$PCL_{19.6}$–$(PEO_{2.0})_4$ (b) and l-$PCL_{6.7}$–$(PEO_{2.0})_2$ (d) copolymers. Heating–cooling cycle: 0–80, 80–0 and 0–80 °C.

the cooling scan. A scan rate of 2 °C/min was selected to obtain a sharp peak separation. Block copolymers with two different crystallisable blocks, such as PCL and PEO, may lead to separate PCL and PEO lamellae within individual crystallites, provided that comparable weight fractions of the two components are present (Jiang et al., 2004). In our case the weight fractions of PEO blocks are 29 and 37 wt.% for s-$PCL_{19.6}$–$(PEO_{2.0})_4$ and l-$PCL_{6.7}$–$(PEO_{2.0})_2$, respectively. Therefore, self-assembly of the investigated amphiphilic copolymers through microphase separation in PCL and PEO crystalline phases was expected. Accordingly, the WAXS diagrams of the copolymers, reported in Fig. 2, exhibited sharp diffraction maxima characteristic of both PCL and PEO crystalline structures at $2\theta = 21.4°$ (PCL) and $2\theta = 19.3°$ (PEO). The broader peak at $2\theta = 23°$–$24°$ arises from the overlapping of the diffraction maxima of PCL at $2\theta = 23.8°$ and PEO at $2\theta = 23.1°$. By taking into account the relative segmental length of PEO and PCL blocks and the melting and crystallization temperatures of the macromers, the high temperature endotherm or exotherm in DSC traces of copolymers were attributed to the melting or crystallization of PCL segments. It is worth remarking that, in spite of their different architecture, s-$PCL_{19.6}$–$PEO_{2.0}$ and l-$PCL_{6.7}$–$PEO_{2.0}$ show similar crystallinities and thermal behaviours. Although the presence of segments of different nature linked each other disturbs the crystallization process, the high tendency of PCL and PEO

Table 2
Thermal properties of PEO and PCL macromers and of ABA triblock and $(BA)_4$ star-diblock copolymers (A = PEO, B = PCL)

Polymer code	T_m[a] (°C)		ΔH_m[a] (J g^{-1})		T_c[a] (°C)		ΔH_c[a] (J g^{-1})		T_g (°C)	X_c[b] (%)
	PEO	PCL	PEO	PCL	PEO	PCL	PEO	PCL		
$PEO_{2.0}$	52 (51)	– –	156 (141)	– –	32	–	139	–	n.d.	n.d.
l-$PCL_{6.7}$	– –	64 (56)	– –	103 (83)	–	41	–	79	−62	75
s-$PCL_{19.6}$	– –	60 (56)	– –	80 (65)	–	37	–	63	−62	60
l-$PCL_{6.7}$–$(PEO_{2.0})_2$	48 (47)	60 (54)	33 (22)	64 (44)	22	36	32	48	−58	57
s-$PCL_{19.6}$–$(PEO_{2.0})_4$	52 (52)	59 (55)	28 (27)	58 (43)	33	40	30	41	−62	51

[a] Melting and crystallization parameters obtained at 2 °C/min rate; the results of second heating runs after cooling from the melt to 0 °C are reported in parenthesis.
[b] Crystallinity degree evaluated from WAXS diagrams.

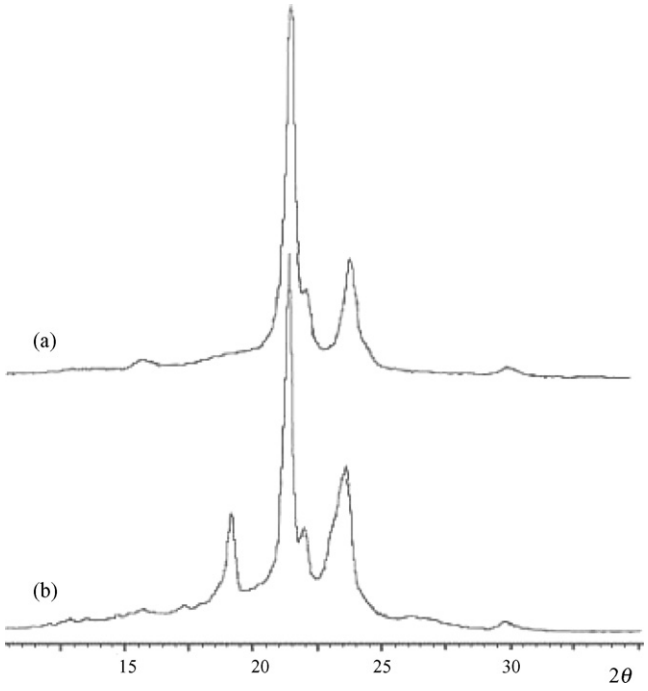

Fig. 2. WAXS diagrams of s-$PCL_{19.6}$ (a) and s-$PCL_{19.6}$–$(PEO_{2.0})_4$ (b).

chains to be arranged in a crystalline structure is preserved in the copolymers, as indicated by the high ΔH_m and X_c values. To better understand the self-association ability of the copolymers in bulk, it was of interest to investigate the morphology of melt crystallized copolymers by polarized optical microscopy. Representative micrographs of s-$PCL_{19.6}$–$(PEO_{2.0})_4$ are shown in Fig. 3. Double spherulites were clearly observed in a melt crystallized sample of the copolymer (a) together with some single spherulites of much smaller size. On the basis of morphologies observed for melt crystallized s-$PCL_{19.6}$ and $PEO_{2.0}$ precursor, the central and the outer portions of double spherulites were assigned to the PCL and PEO components, respectively. In a second heating run, PEO spherulites melted at lower temperature, 52 °C, as shown in Fig. 3b, while PCL spherulites were still observable and melted at 56 °C. These results are in good agreement with those obtained by DSC and indicate that PCL segments crystallize first on cooling from the melt and that their crystallites may act as nucleating agent for the growth of PEO spherulites. A similar behaviour was observed for l-$PCL_{6.7}$–$PEO_{2.0}$. As double spherulitic morphologies were previously reported for PCL–PEO–PCL (Shiomi et al., 2001) and PEO–PCL–PEO (Signori et al., 2005) triblock copolymers, it appears that development of such morphologies may be considered a general feature of PCL–PEO block copolymers, inde-

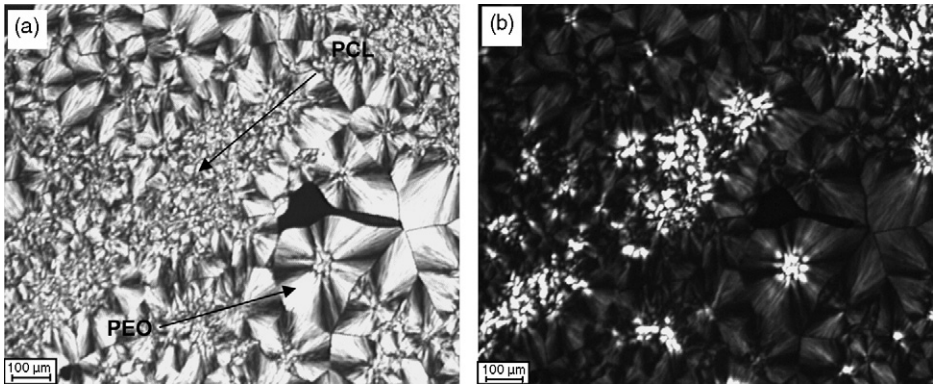

Fig. 3. Polarized optical micrographs of melt crystallized s-$PCL_{19.6}$–$(PEO_{2.0})_4$ copolymer at 25 °C (a) and 52 °C when melting of PEO spherulites occurs (b).

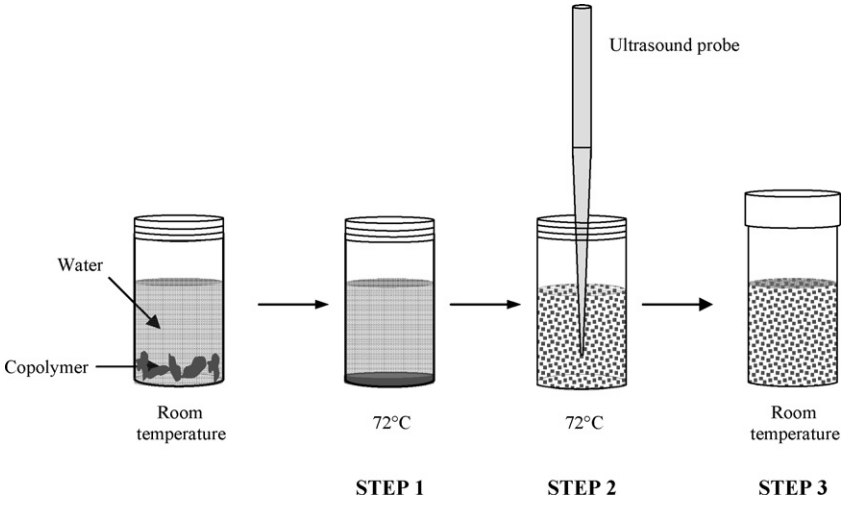

Fig. 4. Steps involved in the preparation of nanoparticles by melting/sonication technique. Step 1: copolymer and water are equilibrated at 72 °C; step 2: the mixture is sonicated; step 3: the sample is cooled at room temperature.

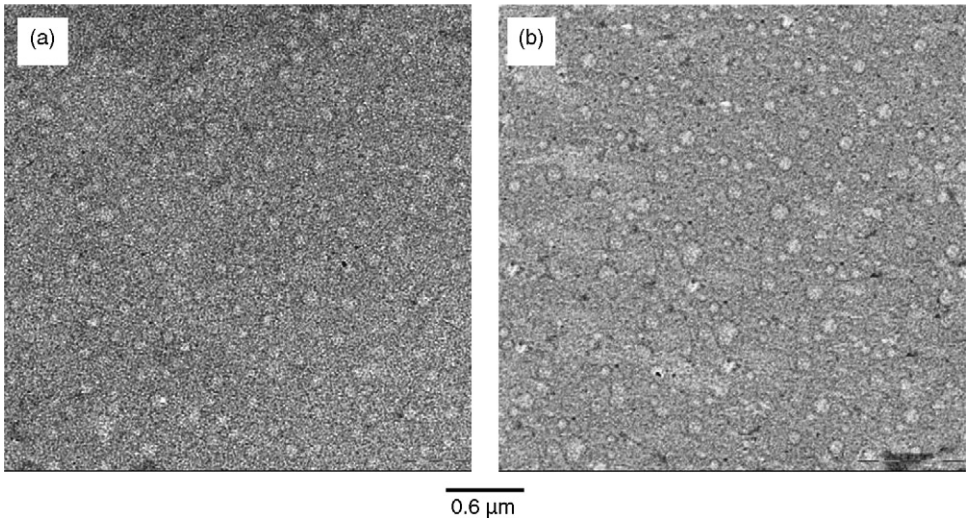

Fig. 5. TEM images of l-$PCL_{6.7}$–$(PEO_{2.0})_2$ nanoparticles (a) and s-$PCL_{19.6}$–$(PEO_{2.0})_4$ nanoparticles (b) made by melting/sonication.

pendently from their architecture, provided that weight fractions and segmental lengths of different blocks are comparable.

3.4. Nanoparticle preparation and characterization

Core-shell nanoparticles were prepared by a reference nanoprecipitation technique (NP) widely employed to produce nanoparticles by interfacial deposition of a polymer following displacement of an organic polar solvent in water. Nanoprecipitation was carried out without the addition of surfactants in the water phase to highlight the surfactant-like properties of the copolymers. Exploiting the rather low melting temperatures and the amphiphilic properties of the block copolymers synthesized, we also tried to develop a novel procedure for nanoparticle preparation, named melting/sonication (MS). The process, schematized in Fig. 4, consists in melting the copolymer in water at a temperature about 10 °C higher than copolymer T_m, applying sonication and then allowing the dispersion to equilibrate at room temperature to promote copolymer hardening. In this way, molten copolymer was supposed to organize spontaneously in nanoscopic core-shell structures due to its amphiphilic and crystallization properties. TEM analysis showed that nanoparticles prepared by MS were spherical and not aggregated (Fig. 5).

Recovery yield, hydrodynamic diameter, polydispersity index and zeta potential of nanoparticles are reported in Table 3. Independently of the fabrication procedure, the recovery yield

Table 3
Some properties of unloaded nanoparticles prepared by nanoprecipitation (NP) and melting/sonication technique (MS)

Polymer code	Technique	Yield (%)	Mean D_H (nm ± S.D.)	PI
l-$PCL_{6.7}$–$(PEO_{2.0})_2$	NP	70	43 ± 3	0.421
	MS	80	92 ± 10	0.199
s-$PCL_{19.6}$–$(PEO_{2.0})_4$	NP	30	96 ± 34	0.390
	MS	12	184 ± 32	0.261

of nanoparticles prepared from l-PCL$_{6.7}$–(PEO$_{2.0}$)$_2$ was higher than that observed for s-PCL$_{19.6}$–(PEO$_{2.0}$)$_4$ suggesting that star architecture is less prone to give core-shell nanocarriers probably due to the higher conformational rigidity. Nanoparticles prepared by MS displayed a hydrodynamic diameter significantly larger than nanoparticles prepared by NP. Monomodal size distributions were observed for all the preparations. No direct comparison between the properties of nanoparticles prepared by different techniques was possible since nanoparticle formation occurs by completely different mechanisms. As a general trend, l-PCL$_{6.7}$–(PEO$_{2.0}$)$_2$ were found to give smaller nanoparticles than s-PCL$_{19.6}$–(PEO$_{2.0}$)$_4$ independently of the technique employed suggesting that copolymer molecular weight, particularly PCL segmental length, affects both its desolvation properties in the NP technique and hot-melt dispersability in the MS technique. It is worth of note that, polydispersity indices of MS nanoparticles were lower as compared to those observed for NP nanoparticles. Independently of the technique employed, nanoparticles were stable upon storage at 4 °C for 30 days, since size did not change significantly and aggregation of the sample was not observed. This result suggests that the concentration of PEO chains on the surface of the particles is high enough to avoid hydrophobic aggregation due to PCL. Zeta potential of PEO–PCL nanoparticles was evaluated at pH 6.5 and 3.0 in media with the same ionic strength (Fig. 6). Zeta potential was negative independently of the technique used for fabrication, probably due to the presence of an ester bond close to the junction point between PEO and PCL where a delocalization of negative charges occurs as well as to the polarization of water molecules under the effect of PEO. Zeta potential values for all the systems were similar demonstrating that both the technique of nanoparticle preparation and copolymer type did not affect the shielding properties of PEO corona. A decrease in medium pH resulted in an increase of zeta potential to more positive values. This result can be reasonably attributed to a different spatial organization of PEO chains on nanoparticles surface and suggests a better steric protection of nanoparticles (Vila et al., 2004) as medium pH decreases.

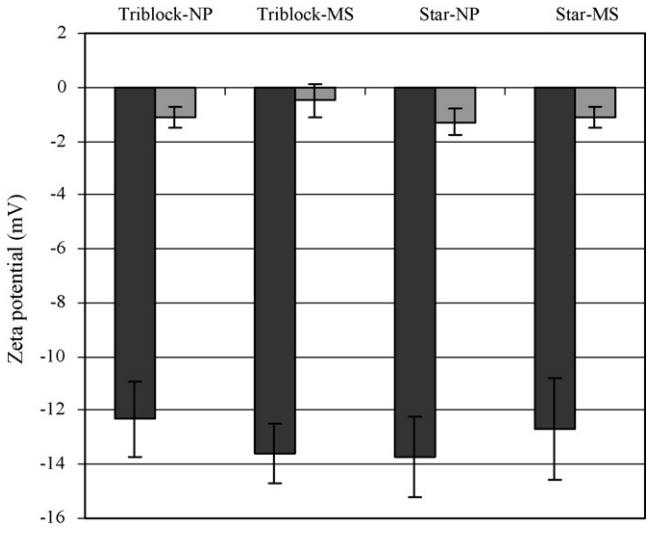

Fig. 6. Zeta potential of unloaded nanoparticles made of l-PCL$_{6.7}$–(PEO$_{2.0}$)$_2$ (triblock) and s-PCL$_{19.6}$–(PEO$_{2.0}$)$_4$ (star) by nanoprecipitation (NP) and melting/sonication (MS) evaluated at pH 6.5 (black bars) and pH 3.0 (grey bars).

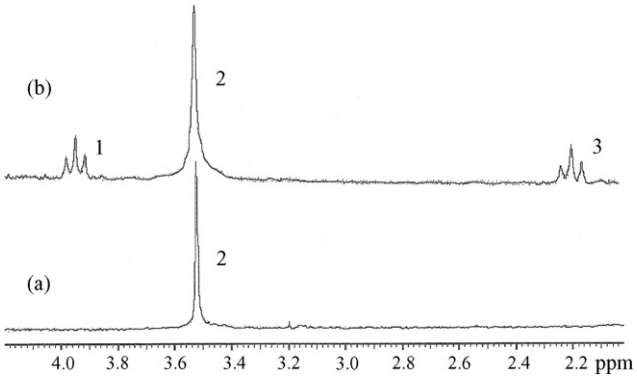

Fig. 7. ^{1}H NMR spectra at 300 MHz of s-PCL$_{19.6}$–(PEO$_{2.0}$)$_4$ in D$_2$O (a) and in chloroform-*d* (b), in the range 4.2–2.0 *δ*. Peak attribution: –CH$_2$–O–CO– of PCL (1), –CH$_2$–O–CH$_2$– of PEO (2), –CH$_2$CO–O– of PCL (3).

The core-shell structure of the nanoparticles prepared by both techniques was confirmed by ^{1}H NMR. The spectrum of s-PCL$_{19.6}$–(PEO$_{2.0}$)$_4$ nanoparticles prepared by MS in D$_2$O (Fig. 7a) was quite different from that obtained by direct dissolution of nanoparticles in chloroform-*d* (Fig. 7b). As chloroform is a good solvent for both PCL and PEO segments, sharp resonances arising from PCL and PEO protons were displayed in the latter spectrum. On the other hand, in D$_2$O, a selective solvent of hydrophilic PEO segments, the proton peaks of PEO moiety were clearly observed as sharp peaks, while those associated to PCL segments were not detected. This finding was attributed to a structural rearrangement of PCL segments driven by hydrophobic interactions, which results in a solid-like structure where the segmental mobility is strongly reduced. Thus, a core-shell structure with highly mobile hydrated PEO segments forming the corona and PCL segments forming a solid-like core, is suggested. Quite analogous results were obtained for nanoparticles of l-PCL$_{6.7}$–(PEO$_2$)$_2$ prepared by the MS technique, as well as for nanoparticles of both copolymers prepared by precipitation of acetone-d_6 solutions in D$_2$O and acetone-d_6 evaporation.

3.5. Properties of atRA-loaded nanoparticles

Encapsulation/release features of nanoparticles were assessed by loading *at*RA, selected as a model compound. Some properties of *at*RA-loaded nanoparticles prepared by both techniques are reported in Table 4. Drug loading by MS technique was achieved by dissolving the drug in a low amount of ethanol. This enabled the lipophilic drug to homogeneously distribute in the aqueous phase and partition in the molten copolymer. It was found that upon *at*RA loading, the PI values were not affected, while the mean D_H slightly decreases except for l-PCL$_{6.7}$–(PEO$_{2.0}$)$_2$ nanoparticles prepared by NP which displayed the lowest D_H. For both techniques, drug contents and loading efficiency increased as the molecular weight of PCL block did. This can be reasonably attributed to the fact that the extent of polymer/drug hydrophobic interactions increases as the length of PCL blocks increases. On the other hand,

Table 4
Some properties of *at*RA-loaded nanoparticles

Polymer code	Preparation technique	Mean D_H (nm ± S.D.)	PI	Zeta potential[a] (mV ± S.D.)	*at*RA actual loading[b] (% ± S.D.)	*at*RA encapsulation. efficiency[c] (% ± S.D.)
l-$PCL_{6.7}$–$(PEO_{2.0})_2$	NP	44 ± 2	0.479	−8.2 ± 0.7	0.20 ± 0.01	2.3 ± 0.05
	MS	60 ± 8	0.178	−3.1 ± 0.7	0.58 ± 0.03	6.4 ± 0.01
s-$PCL_{19.6}$–$(PEO_{2.0})_4$	NP	70 ± 10	0.371	−6.2 ± 1.9	0.57 ± 0.01	6.3 ± 0.03
	MS	144 ± 23	0.391	−3.8 ± 1.2	0.86 ± 0.02	9.5 ± 0.01

[a] Zeta potential measurements were performed in 0.02 M phosphate buffer at pH 6.5.
[b] Actual loading is expressed as the amount of *at*RA emcapsulated per 100 mg of nanoparticles.
[c] Ratio between actual and theoretical loading × 100. Theoretical loading was 10%.

particle size can also play a role since it seems directly related to the amount of *at*RA encapsulated, as already demonstrated for similar nanoparticles by Jeong et al. (2004). Zeta potential of *at*RA-loaded nanoparticles (Table 4) was more positive than that of the unloaded nanoparticles. Since *at*RA is negatively ionized at pH 6.5, this result suggests that its ionic charge does not contribute to zeta potential values. Therefore, the increase of zeta potential for *at*RA-loaded nanoparticles can be assumed to be mainly contributed by the different organization of PEO chains in the external corona consequent to drug incorporation which results in a better steric protection of the nanoparticles. This hypothesis is further supported by the fact that a decrease in medium pH, while maintaining the same ionic strength, produced an increase of zeta potential (data not shown) as for unloaded nanoparticles.

The release profiles of *at*RA from nanoparticles are reported in Fig. 8. For each type of copolymer *at*RA release was faster from nanoparticles prepared by MS. Furthermore, release of *at*RA occurred at similar rates for nanoparticles obtained by MS whereas, in the case of NP technique, the release from s-$PCL_{19.6}$–$(PEO_{2.0})_4$ nanoparticles was much slower than that observed for l-$PCL_{6.7}$–$(PEO_{2.0})_2$ nanoparticles. It has been demonstrated that nanoparticles made of PCL–PEO diblock

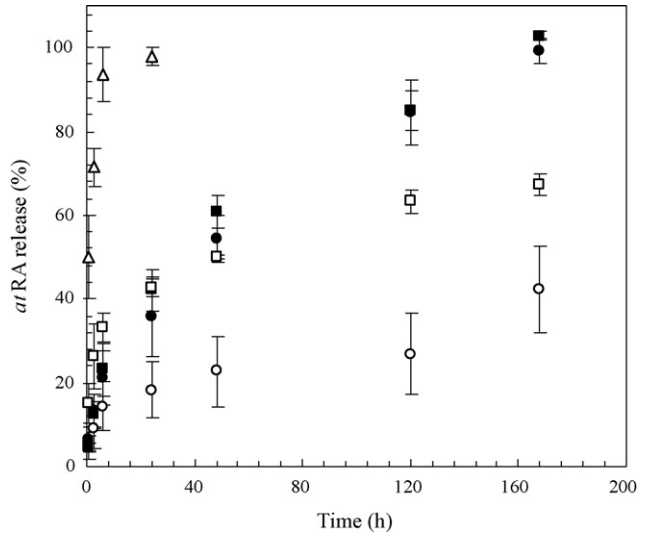

Fig. 8. Release profiles of *at*RA in 10 mM phosphate buffer pH 7.4 and 37 °C. Nanoprecipitated *at*RA (△), l-$PCL_{6.7}$–$(PEO_{2.0})_2$ nanoparticles (■, □), s-$PCL_{19.6}$–$(PEO_{2.0})_4$ nanoparticles (●, ○). Nanoprecipitation technique (open symbols), melting/sonication technique (solid symbols).

copolymers with a molecular weight lower than that of the copolymers reported in this study degrade very slowly in aqueous environments, the extent of degradation being about 4% after 10 days (Jeong et al., 2004). This means that release mechanism can be assumed mainly dominated by diffusion in the time framework of our experiment. Therefore at least four aspects contribute to release profiles, that is permeability of the polymer matrix to the diffusing drug, nanoparticle size, actual loading and dissolution properties of the drug in the medium hydrating the nanoparticles. This last phenomenon has been highlighted for nanoparticles prepared by NP, and attributed to the fact that a part of the drug, especially at high loadings, can crystallize inside nanoparticles upon phase separation (Gref et al., 1994). On the basis of the results reported by Jeong et al. (2004), who observed *at*RA crystallization inside nanoparticles made of PCL–PEO diblock copolymers at *at*RA loadings much higher than those realized in our study, we excluded any crystallization of the drug inside the nanoparticles. Release kinetics for nanoparticle prepared by MS was faster than that obtained from nanoparticles prepared by NP, although MS nanoparticles had a larger size and were expected to release the drug more slowly. It is our opinion, that the different mechanisms of nanoparticle formation and drug loading are the main determinant for drug release rate. In the case of NP process a progressive desolvation of the polymer occurs whereas in MS technique, nanoparticles are formed from a molten copolymer by crystallization. On the other hand also loading process is different, consisting in a progressive desolvation of drug/polymer for NP whereas a drug partitioning in the molten copolymer takes place for MS technique. This last effect can result in a different distribution of the drug in MS nanoparticles, being the drug preferentially located in the outer layer and thus released more rapidly. The fact that differences between release rates for nanoparticles prepared by different copolymer types were evident only in the case of NP technique further support this view. In this last case, a longer pathway for drug diffusion in the polymer matrix for NP nanoparticles highlights the contribution of core hydrophobicity on drug release rate.

3.6. Studies on complement activation of l-$PCL_{6.7}$–$(PEO_{2.0})_2$ and s-$PCL_{19.6}$–$(PEO_{2.0})_4$ nanoparticles prepared by melting/sonication

It has been widely demonstrated that PEO-coated nanoparticles have the potential to escape RES due to the presence of a hydrophilic coating, which limits carrier opsonization and thus

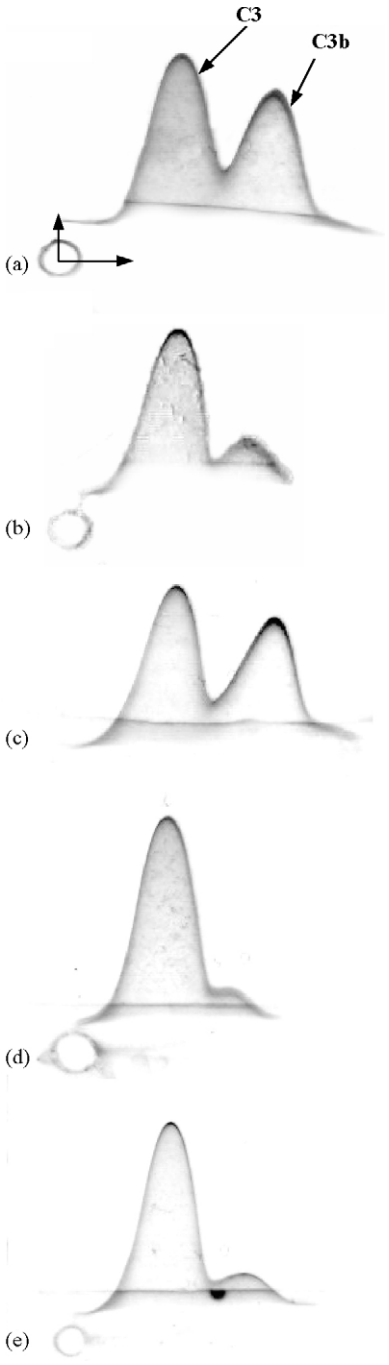

Fig. 9. Crossed immunoelectrophoresis of C3 antigens in human serum diluted in VBS^{2+} after 1 h incubation with nanoparticle suspension at constant surface area (1000 cm^2). (a) Sephadex G25 (positive control); (b) serum/VBS^{2+} (negative control); (c) PCL nanoparticles; (d) l-$PCL_{6.7}$–$(PEO_{2.0})_2$ nanoparticles; (e) s-$PCL_{19.6}$–$(PEO_{2.0})_4$ nanoparticles. Nanoparticles of PEO–PCL were prepared by melting sonication.

recognition and clearing up by RES macrophages. An efficient method to understand if an intravenously injected nanocarrier can cause complement activation and aspecific recognition consists in measuring the extent of complement activation. Protein C3 is a major plasma protein of the complement system circulating in functionally inactive form and involved in the non-specific recognition, i.e. opsonization, of foreign bodies. A critical step of complement activation consists in the cleavage of C3 into a large fragment C3b and a small fragment C3a. 2D immunoelectrophoresis of C3 and C3b performed to evaluate the degree of complement activation induced by the nanoparticles after incubation in serum containing calcium and magnesium ions are illustrated in Fig. 9. Independently of the copolymer employed and preparation technique, nanoparticles showed almost the same pattern than the negative control, thus suggesting that no complement activation occurred. Gref et al. (2000) have shown in a detailed study that a $PEO_{5.0}$ coating results in a maximal reduction of protein adsorption on PEO/PLA nanoparticles and a PEO content between 2 and 5% can be considered a threshold value to limit protein adsorption. Furthermore, core nature of nanoparticles is another important factor in affecting the quality and amount of adsorbed properties. Our results demonstrate that, independently of the nature of proteins adsorbed, nanoparticles based on s-$PCL_{19.6}$–$(PEO_{2.0})_4$ or l-$PCL_{6.7}$–$(PEO_{2.0})_2$ prepared by the novel MS technique do not activate complement although PEO chains were shorter and are in agreement with the recent findings of Vonarbourg et al. (2006) on pegylated lipid nanocapsules. Thus, copolymer architectures proposed in this study can be of great interest in the development of long-circulating nanocarriers.

4. Conclusions

In this work it has been shown that amphiphilic copolymers with triblock and star-diblock architectures are suitable for applications in nanoparticle technology. Nanoparticles can be prepared by the classical nanoprecipitation technique and by a novel procedure, named melting/sonication, making use of the quite low melting temperature of PEO–PCL copolymers. Nanoparticles prepared by melting/sonication have a core-shell structure, with a PEO coating on the surface, do not activate complement, can incorporate lipophilic drugs and do not show burst release. Finally, our results suggest that the nanocarriers developed are of interest in the delivery of drugs through EPR effect.

Acknowledgements

The authors would like to thank Dr. Emilia Di Pace (Istituto di Chimica e Tecnologia dei Polimeri, CNR) for optical microscopy experiments and the CIMCF Centre of Federico II University for NMR facilities. The financial support of MIUR (PRIN 2005) is gratefully acknowledged.

References

Bhadra, D., Bhadra, S., Jain, P., Jain, N.K., 2002. Pegnology: a review of PEGylated systems. Pharmazie 57, 5–29.

Brannon-Peppas, L., Blanchette, J.O., 2004. Nanoparticle and targeted systems for cancer therapy. Adv. Drug Deliv. Rev. 56, 1649–1659.

Couvreur, P., Vauthier, C. Nanotechnology: intelligent design to treat complex disease. Pharm. Res. 2006.

Emerich, D.F., Thanos, C.G., 2003. Nanotechnology and medicine. Expert Opin. Biol. Ther. 3, 655–663.

Fessi, H., Devissaguet, J.P., Puisieux, F., Thies, C., 1986. French Patent 2,608,988.

Gref, R., Luck, M., Quellec, P., Marchand, M., Dellacherie, E., Harnisch, S., Blunk, T., Muller, R.H., 2000. 'Stealth' corona-core nanoparticles surface modified by polyethylene glycol (PEG): influences of the corona (PEG chain length and surface density) and of the core composition on phagocytic uptake and plasma protein adsorption. Colloids Surf. B Biointerf. 18, 301–313.

Gref, R., Minamitake, Y., Peracchia, M.T., Trubetskoy, V., Torchilin, V., Langer, R., 1994. Biodegradable long-circulating polymeric nanospheres. Science 263, 1600–1603.

Jain, K.K., 2005. Nanotechnology in clinical laboratory diagnostics. Clin. Chim. Acta 358, 37–54.

Jeong, Y.I., Kang, M.K., Sun, H.S., Kang, S.S., Kim, H.W., Moon, K.S., Lee, K.J., Kim, S.H., Jung, S., 2004. All-trans-retinoic acid release from core-shell type nanoparticles of poly(epsilon-caprolactone)/poly(ethylene glycol) diblock copolymer. Int. J. Pharm. 273, 95–107.

Jiang, S., He, C., An, L., Chen, X., Jiang, B., 2004. Crystallization and ring-banded spherulitic morphology of poly(ethylene oxide)-block-poly(epsilon-caprolactone) diblock copolymers. Macromol. Chem. Phys. 205, 2234.

Kim, C.K., Lim, S.J., 2002. Recent progress in drug delivery systems for anti-cancer agents. Arch. Pharm. Res. 25, 229–239.

Kim, D., El Shall, H., Dennis, D., Morey, T., 2005. Interaction of PLGA nanoparticles with human blood constituents. Colloids Surf. B Biointerf. 40, 83–91.

Kumar, N., Ravikumar, M.N., Domb, A.J., 2001. Biodegradable block copolymers. Adv. Drug Deliv. Rev. 53, 23–44.

Labarre, D., Vauthier, C., Chauvierre, C., Petri, B., Muller, R., Chehimi, M.M., 2005. Interactions of blood proteins with poly(isobutylcyanoacrylate) nanoparticles decorated with a polysaccharidic brush. Biomaterials 26, 5075–5084.

Lemarchand, C., Couvreur, P., Besnard, M., Costantini, D., Gref, R., 2003. Novel polyester-polysaccharide nanoparticles. Pharm. Res. 20, 1284–1292.

Lemarchand, C., Gref, R., Couvreur, P., 2004. Polysaccharide-decorated nanoparticles. Eur. J. Pharm. Biopharm. 58, 327–341.

Maglio, G., Nese, G., Nuzzo, M., Palumbo, R., 2004. Synthesis and characterization of star-shaped diblock poly(epsilon-caprolactone)/poly(ethylene oxide) copolymers. Macromol. Rapid Commun. 25, 1139–1144.

Moghimi, S.M., Hunter, A.C., Murray, J.C., 2005. Nanomedicine: current status and future prospects. FASEB J. 19, 311–330.

Otsuka, H., Nagasaki, Y., Kataoka, K., 2003. PEGylated nanoparticles for biological and pharmaceutical applications. Adv. Drug Deliv. Rev. 55, 403–419.

Qiu, L.Y., Bae, Y.H., 2006. Polymer architecture and drug delivery. Pharm. Res. 23, 1–30.

Reddy, L.H., 2005. Drug delivery to tumours: recent strategies. J. Pharm. Pharmacol. 57, 1231–1242.

Shiomi, T., Imai, K., Takenaka, K., Takeshita, H., Hayashi, H., Tezuka, Y., 2001. Appearance of double spherulites like concentric circles for poly(-caprolactone)-block-poly(ethylene glycol)-block-poly(-caprolactone). Polymer 42, 3239.

Signori, F., Chiellini, F., Solaro, R., 2005. New self-assembling biocompatible-biodegradable amphiphilic block copolymers. Polymer 46, 9652.

Soppimath, K.S., Aminabhavi, T.M., Kulkarni, A.R., Rudzinski, W.E., 2001. Biodegradable polymeric nanoparticles as drug delivery devices. J. Control. Release 70, 1–20.

Vasir, J.K., Labhasetwar, V., 2005. Targeted drug delivery in cancer therapy. Technol. Cancer Res. Treat. 4, 363–374.

Vila, A., Gill, H., McCallion, O., Alonso, M.J., 2004. Transport of PLA–PEG particles across the nasal mucosa: effect of particle size and PEG coating density. J Control. Release 98, 231–244.

Vonarbourg, A., Passirani, C., Saulnier, P., Simard, P., Leroux, J.C., Benoit, J.P., 2006. Evaluation of pegylated lipid nanocapsules versus complement system activation and macrophage uptake. J. Biomed. Mater. Res. A 2006.